

Flexible Synthesis of Bio-Hydroxyapatite/Chitosan Hydrogel Beads for Highly Efficient Orange G Dye Removal: Batch and Recirculating Fixed-Bed Column Study

Bouthayna Kjidaa,* Zaineb Mchich, Khalid Aziz, Nabil Saffaj, Taoufiq Saffaj, and Rachid Mamouni*



Cite This: *ACS Omega* 2024, 9, 8543–8556



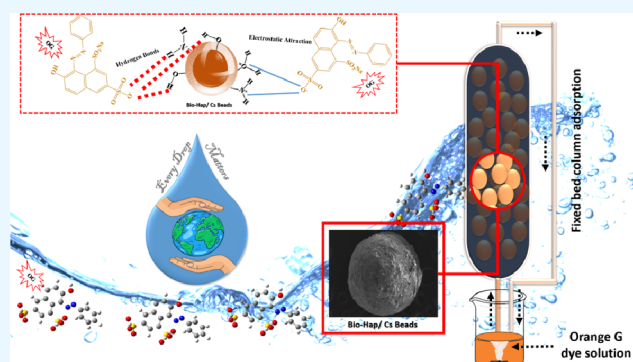
Read Online

ACCESS |

Metrics & More

Article Recommendations

ABSTRACT: The use of fish waste as a source material for the development of functional beads has significant potential applications in the fields of materials science and environmental sustainability. In this study, a biomaterial bead of chitosan was cross-linked with bio-hydroxyapatite (Bio-Hap/Cs) through the encapsulation process to create a stable and durable material. The beads are characterized using scanning electron microscopy combined with energy dispersive X-ray spectrometry, Fourier transform infrared spectroscopy, and X-ray diffraction techniques. The adsorption efficiency of Bio-Hap/Cs hydrogel beads was evaluated by using Orange G (OG) dye in both batch and recirculating column systems, and the effect of various parameters on the adsorption capacity was investigated. In the batch study, it was found that OG removal increased with an increasing pH and adsorbent dose. However, in the recirculating column system, a higher bed height and lower flow rate led to increased removal of the OG dye. The kinetic study indicated that the pseudo-second-order model provided a good description of OG adsorption onto Bio-Hap/Cs beads in both batch and recirculating processes, with a high coefficient correlation. The maximum adsorbed amounts are found to be 19.944 mg g⁻¹ and 9.472 mg g⁻¹ in batch and recirculating processes, respectively. Therefore, Bio-Hap/Cs hydrogel beads have demonstrated an effective and reusable material for OG dye remediation from aqueous solutions using recirculating adsorption processes.



1. INTRODUCTION

In recent decades, many industries, including textile, paper, leather, and printing, have used large quantities of synthetic dyes, resulting in widespread environmental contamination.^{1,2} The dyes, such as azo, reactive, acidic, alkaline, and neutral, found in industrial effluents exhibit persistent resistance to biodegradation and pose significant risks to the health of aquatic organisms and humans, exhibiting toxic, teratogenic, carcinogenic, and mutagenic effects. Addressing these problems and discovering appropriate preventive measures generally take a considerable amount of time.³ To mitigate and prevent dye pollution, several treatment methods have been implemented to clean up colored effluents, such as coagulation-flocculation,⁴ photocatalysis,⁵ membrane filtration,⁶ and adsorption.^{7,8} Nevertheless, the adsorption process is considered to be an effective and simple method that is relatively free from the concerns of generating unwanted byproducts and has a good percentage of dye removal. The main benefits of adsorption process include their simplicity, highly cost-effective and economically energy consumption, environmental friendliness, and recyclability.^{9,10}

Numerous studies are being conducted to discover low-cost, eco-friendly materials to eliminate pollutants in aqueous environments.¹¹ Crucial importance has been gained on the biomaterials as adsorbents to remove contaminants, which can reduce the process cost substantially and make the adsorption method more ecological and feasible.¹² The encapsulated materials have gained significant attention in recent years as effective adsorbents for the removal of dyes from wastewater.¹³ These materials have the ability to trap active agents within their structures, which enhances their stability, reusability, and selectivity. The use of encapsulated materials for column applications is a promising approach for the dye elimination from wastewater and has the potential to significantly reduce the environmental impact of textile and dyeing industries.¹⁴

Received: December 15, 2023

Revised: January 19, 2024

Accepted: January 24, 2024

Published: February 7, 2024



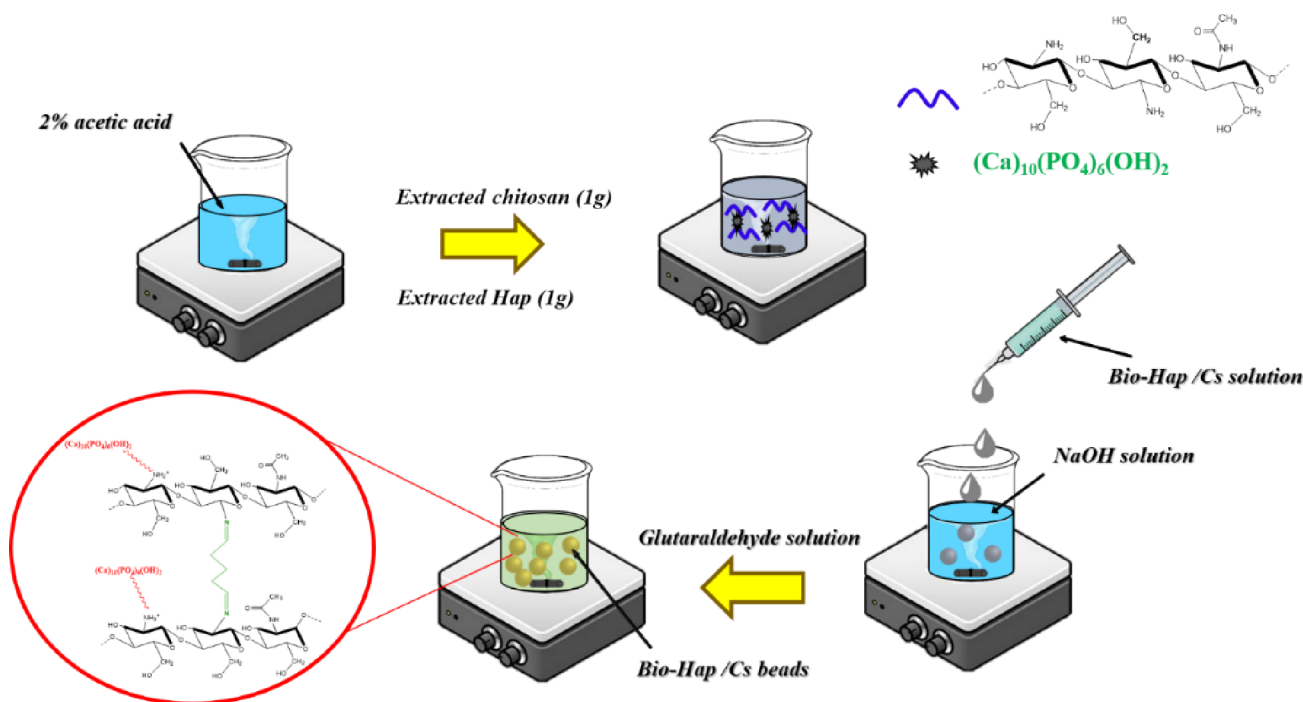


Figure 1. Cross-linking protocol for the bio-Hap/Cs hydrogel beads preparation.

To improve the efficiency of purification, separation, and recovery of target compounds in industrial-scale applications, a continuous adsorption system using material beads in column reactors has several advantages over conventional water treatment methods.¹⁵ Chitosan (Cs) is widely recognized as one of the most popular adsorbents for dye removal. Cs, originates from chitin, a bioactive polymer known for its remarkable antimicrobial properties. This naturally derived material is cost-effective, environmentally benign, and biodegradable and demonstrates low toxicity. Chitosan beads are commonly employed in batch mode, owing to their high adsorption capacity, rapid kinetics, and cost efficiency. However, their application may encounter limitations due to their low mechanical strength and susceptibility to acid solubility.^{16,17} To overcome these limitations, researchers have been actively exploring methods to enhance the polymer matrix, aiming to create a composite material that is adaptable and versatile in various functions groups. An integral method involves utilizing glutaraldehyde (GA) to cross-link chitosan, forming covalent bonds that address chitosan's inherent solubility challenges and reinforce the composite's structural integrity. Additionally, incorporating an inorganic matrix into the polymer structure functions as a mechanism to introduce a diverse range of functional groups. Hydroxyapatite (Hap), an inorganic matrix, has been effectively employed to create these hybrids for environmental applications. Moreover, its extraction from natural biological resources such as eggshells, bovine bones, and fish scales presents an eco-friendlier and cost-effective alternative compared to chemical synthesis processes.^{18,19}

In the present study, we have designed a novel adsorbent for Orange dye immobilization using the encapsulation process of fish scales cross-linked chitosan biopolymer. A facile synthesis of crystalline bio-hydroxyapatite (Bio-Hap) was performed via alkaline heat treatment of fish scale bioresource in the aqueous phase. The prepared bio-hydroxyapatite/chitosan (Bio-Hap/

Cs) hydrogel beads were characterized using SEM-EDS, XRD, and FTIR analysis. The performance of these newly prepared beads for removing OG dye was studied by using batch adsorption experiments and a recirculating column process that acted as a practical sorbent. Finally, the regeneration study was conducted to assess the reusability of the Bio-Hap/Cs hydrogel beads in fixed bed column.

2. MATERIALS AND METHODS

2.1. Chemicals. The fish scales and shrimp shells were collected from a fish market in Agadir (Morocco). The chemical and reagent used, including hydrochloric acid (HCl, 37%), acetic acid, sodium hydroxide (NaOH, pellets), and Orange G (OG) dye, were purchased from Sigma-Aldrich, and glutaraldehyde (25%) was supplied by Fluka.

2.2. Bio-Hydroxyapatite and Chitosan Polymer Extraction. In a previous investigation, the natural hydroxyapatite used in this research was derived from fish scales through an alkaline heat treatment process.²⁰ The fish scales were initially cleaned using tap water and deionized water, followed by drying them at 60 °C for a period of 3 h. Next, the scales were immersed in a hydrochloric acid solution (0.1 M) for 1 h to eliminate any organic substances. Afterward, the scales were thoroughly washed with distilled water and subjected to agitation in a sodium hydroxide solution (5% w/v) at 60 °C for 12 h. This procedure resulted in the formation of a white precipitate, which was subsequently filtered, rinsed with deionized water until neutralized, and finally dried in an oven overnight at 100 °C.

The process of obtaining the biopolymer from shrimp shells involved several stages. The shells were thoroughly washed with boiling deionized water to remove all fats and impurities. Then, the shells were air-dried and ground to a particle size of less than 80 μm. Chemical isolation of chitin and chitosan was performed in four steps: first, the shells are continuously agitated for 24 h in a solution of HCl (7%v/v) to remove

Table 1. Equations and Parameter Specifications for Isotherm, Kinetic, and Thermodynamic Models

		equations	parameters description	reference
nonlinear kinetic models	PFO	$Q_t = Q_e(-\exp(-k_1 t))$	Q_t adsorbed quantity at instant t (min), k_2 ($\text{kg g}^{-1} \text{min}^{-1}$) constant rate of PSO and k_1 (min^{-1}) constant rate of PFO	23,24
	PSO	$Q_t = \frac{Q_e^2 k_2 t}{1 + Q_e k_2 t}$		
nonlinear isotherm models	Langmuir	$Q_e = \frac{Q_{\max} K_L C_e}{1 + K_L C_e}$	Q_e (mg g^{-1}) represents adsorbed quantity at equilibrium, C_e (mg L^{-1}) refers to concentration at equilibrium, K_F is Freundlich constant, K_L is Langmuir constant, n defined adsorption intensity which ($2 < n < 10$) good adsorption, ($1 < n < 2$) moderately difficult, ($n < 1$) adsorption poor	25,26
	Freundlich	$Q_e = K_F C_e^{1/n}$		
thermodynamic study	Gibbs free energy	$\Delta G = \Delta H - T\Delta S$	T is temperature (K) ΔS ($\text{J mol}^{-1} \text{K}^{-1}$) entropy change, ΔG (kJ mol^{-1}) Gibbs free energy change, and ΔH (kJ mol^{-1}) enthalpy change. K_d is distribution coefficient. Q_m is adsorbed amount (mg g^{-1}). R constant of gas and C_e concentration dye at equilibrium	27,28
	Van't Hoff	$\ln K_d = \frac{\Delta S}{R} - \frac{\Delta H}{RT}$		
		$K_D = \frac{Q_m}{C_e}$		

inorganic CaCO_3 (demineralization). Afterward, under stirred conditions for 24 h, 10% sodium hydroxide solution is used to eliminate proteins (deproteinization). The small amounts of pigment can be removed using 95% ethanol (decoloration and bleaching). All or part of the acetylated groups on the obtained chitin are removed chemically during the deacetylation process to produce chitosan. In this step, chitin was hydrolyzed with 50% (w/v) NaOH in an alkaline medium and stirred at a fixed temperature of 110 °C for 4 h. The resultant mixture was filtered and neutralized with hot deionized water at 60 °C. The chitosan was then stored in airtight containers.²¹

2.3. Biocomposite Beads Preparation. The encapsulated Bio-Hydroxyapatite (Bio-Hap) cross-linked chitosan (Cs) biomaterial beads were prepared by the following process. First, a solution of chitosan was prepared by dissolving 1 g of extracted chitosan powder in 2% acetic acid. Next, the chitosan solution was mixed with 1 g of extracted Bio-Hap powder and continuously stirred for 6 h. For beads preparation, the homogeneous mixture was continuously dispensed using a syringe into a solution of NaOH (2% w/v) and stirred for 3 h. The obtained beads were then washed several times with distilled water until they reached neutral pH and immersed in a glutaraldehyde solution for 12 h. Finally, the synthesized Bio-Hydroxyapatite/Chitosan (Bio-Hap/Cs) hydrogel beads were rinsed with distilled water and retained in a distilled water solution. A schematic representation of the Bio-Hap/Cs biocomposite beads synthesis process is provided in Figure 1.

2.4. Characterization Techniques. The identification of functional groups present in the biocomposite beads was conducted through Fourier transform infrared (FTIR) analysis using an ALPHA Bruker Optics instrument located in Germany. In order to obtain the X-ray diffraction (XRD) patterns of the powdered samples, an EMPYREAN PAN-ALYTICAL diffractometer was employed, operating in the 2θ range from 5° to 60° with Cu $K\alpha$ radiation (40 kV and 25 mA) and a scan step of 0.05°. Scanning electron microscopy (SEM) utilizing a JEOL JSM-IT200 instrument was employed to capture micrographs of the Bio-Hap/Cs biocomposite beads before and after adsorption. Additionally, elemental composition analysis was performed by using energy dispersive X-ray spectrometry (EDS).

Our approach to determining the size distribution of the biocomposite beads involved measuring each bead individually, adhering rigorously to standard measurement practices. This thorough process encompassed examining over 20 beads; each bead underwent three measurements to account for potential

variations, and the average diameter was calculated. This detailed approach significantly contributed to our understanding of the observed size distribution.

The method used to determine the point of zero charge (pH_{PZC}) involved adding 20 mg of adsorbent beads to a 20 mL NaCl solution (0.05 M) with pH levels ranging from 3 to 12. The mixture was stirred for 24 h at 25 °C, and the final pH value (pH_f) of the solutions was measured. The value of pH_{PZC} represents the specific point at which the curve depicting the difference in pH (ΔpH , calculated as $\text{pH}_f - \text{pH}_i$) plotted against the initial pH (pH_i) intersects the zero line.¹⁸

2.5. Static and Dynamic Adsorption Process. The batch adsorption experiments were conducted to evaluate the effect of various factors on the adsorptive potentials of the adsorbent. The effect of adsorbent dose was performed by varying the dosage between 0.25 and 3 g L^{-1} . To examine the influence of pH on the adsorption process, the pH values were varied from 3 to 12. The impact of contact time was studied by exposing 20 mg of the adsorbent to 20 mL of a specified OG dye concentration (20 mg L^{-1}), with durations ranging from 5 to 180 min. Lastly, the adsorption process of the OG dye was investigated by varying the OG dye initial concentration from 20 to 220 mg L^{-1} .

The typical Bio-Hap/Cs beads with an average size of 2 mm were used in a recirculating fixed bed column. The fixed-bed adsorption analysis was performed by using a column with a length of 10 cm and an inner diameter of 1.5 cm. The flow rates of 2, 3, and 4 mL min^{-1} , OG dye initial concentration from 5 to 80 mg L^{-1} , and column bed heights of 1, 3, and 5 cm were adopted in the present research work to study the effect of OG dye adsorption performance and to establish optimal conditions in a recirculating fixed bed column by Bio-Hap/Cs beads. The samples were collected and analyzed with a UV spectrophotometer at 476 nm.

In order to calculate the adsorption amount Q_e (mg g^{-1}) and percentage removal R (%) for static and dynamic adsorption, the following equations were used:²²

$$R\% = \left(1 - \frac{C_e}{C_0}\right) \times 100 \quad (1)$$

$$Q_e = \frac{C_0 - C_e}{m} \times V \quad (2)$$

The initial and final concentrations of the OG dye solution are C_0 and C_e , respectively. While, m (g) is the biobeads dose, and V (L) is the dye solution volume.

Table 2. Experimental Levels for OG Adsorption on Bio-Hap/Cs Hydrogel Beads

factor	symbol	units	level				
			-r	-1	0	+1	+r
adsorbent dose	X_{AD}	g L^{-1}	6.591	10	15	20	23.409
concentration of OG dye	X_{OG}	mg L^{-1}	11.591	15	20	25	28.409
contact time	X_{CT}	min	99.546	120	150	180	200.454

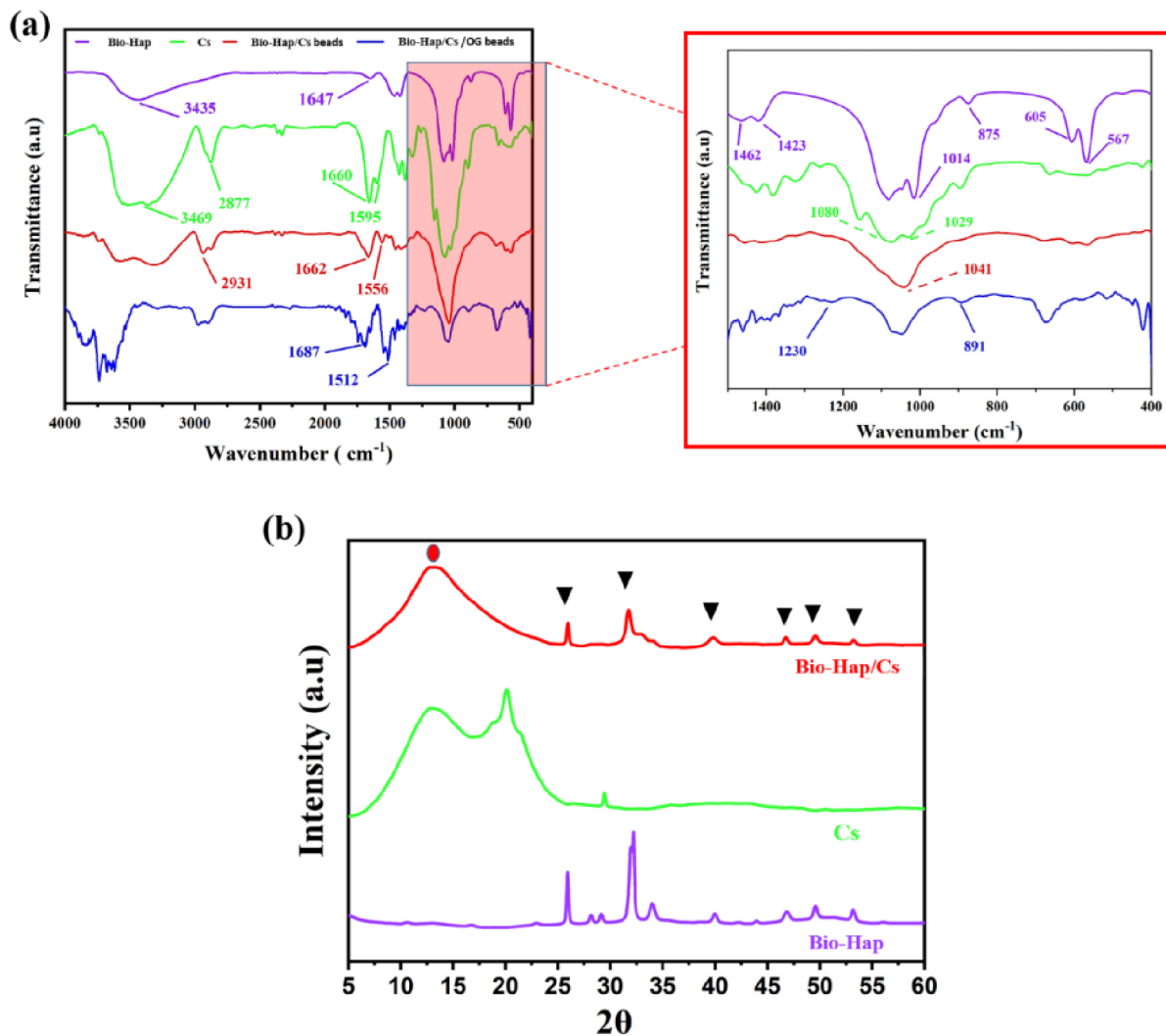


Figure 2. FTIR spectra of Bio-Hap, Cs, and Bio-Hap/Cs hydrogel beads before and after adsorption (a); (b) XRD patterns of Hap, Cs, and Bio-Hap/Cs beads.

2.6. Theoretical Equations for the Adsorption Process. To describe the kinetic mechanism of OG dye interaction with hydrogel beads, the study explored the nonlinear pseudo-second-order (PSO) and pseudo-first-order (PFO) models. In addition, the adsorption equilibrium data of OG dye molecules on Bio-Hap/Cs beads were assessed by using Freundlich and Langmuir isotherms to investigate the adsorption mechanism. Table 1 presents the mathematical equations corresponding to the applied models used to fit the experimental outcomes.

2.7. Optimization Study. Response surface methodology based on central composite design (RSM-CCD) was applied to improve the adsorption of OG dye on Bio-Hap/Cs hydrogel beads by optimizing the controlling factors. The design included three variable factors, namely, X_{AD} (adsorbent

mass), X_{OG} (Orange G concentration (OG)), and X_{CT} (contact time), which were selected from pretests and optimized using a complete design consisting of five levels (-r, -1, 0, +1, +r). The ranges and levels of the different factors are shown in Table 2. This approach resulted in the development of a second-order mathematical equation that establishes a relationship between the adsorption efficiency and the influencing variables of OG.

$$Y = a_0 + \sum_{i=1}^k a_i X_i + \sum_{i=1}^K a_{ii} X_i^2 + \sum_{i=1}^k \sum_{j=1}^K a_{ij} X_i X_j + \varepsilon \quad (3)$$

Y is the predicted result (removal, %); X_j and X_i are the coded values of independent variables; a_i , a_{ij} , and a_{ii} are the

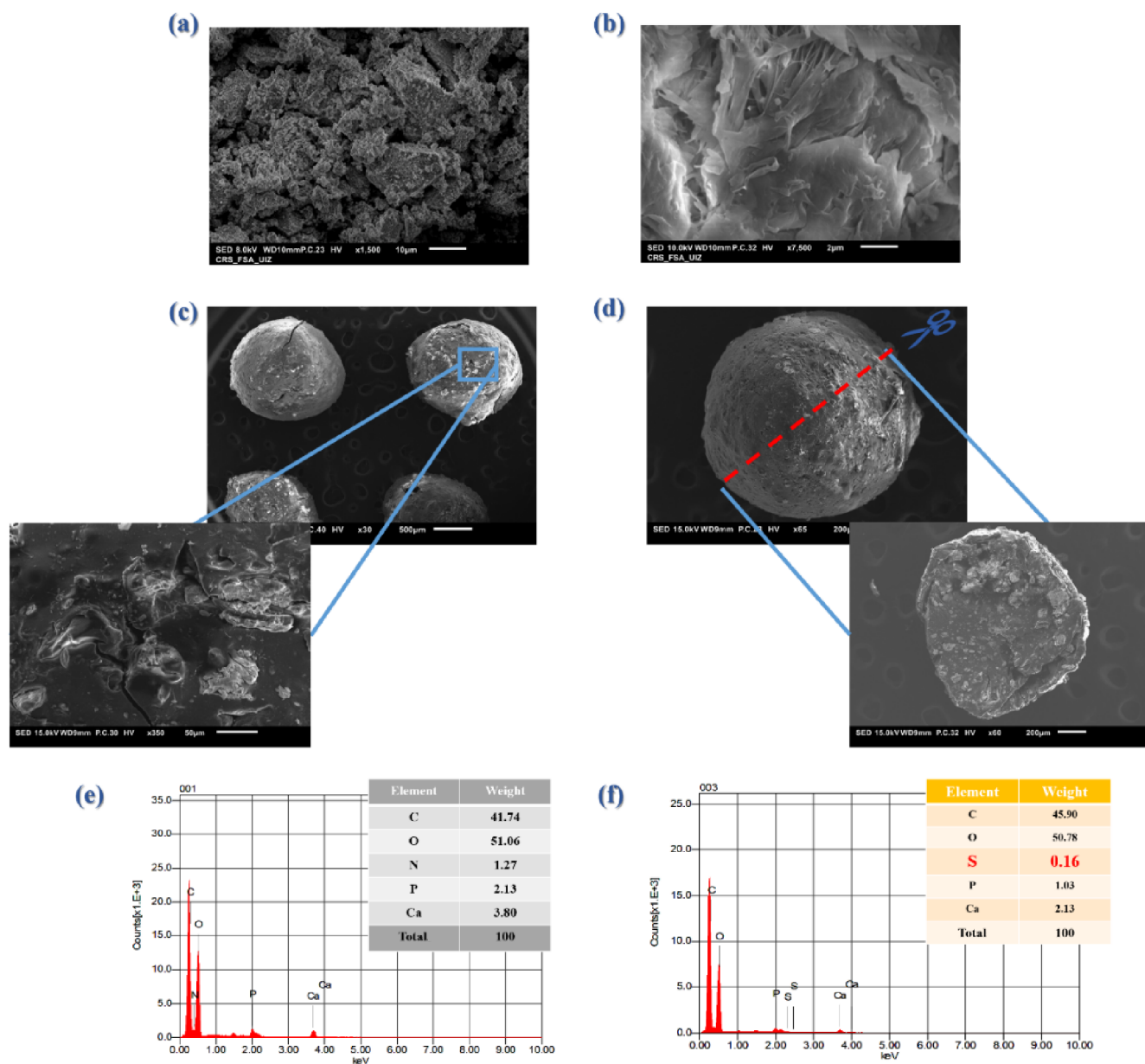


Figure 3. SEM micrographs of Bio-Hap (a), Cs (b), and Bio-Hap/Cs beads (c) before and (d) after adsorption. EDS elemental analysis of Bio-Hap/Cs beads (e) before and (f) after adsorption.

linear, interaction, and quadratic coefficients; and a_0 is constant.

3. RESULTS AND DISCUSSION

3.1. Characterizations. Figure 2a depicts the FTIR spectra of Bio-Hap, Cs, and Bio-Hap/Cs beads. A Bio-Hap spectrum shows vibrations at 875 cm^{-1} and $1100\text{--}962\text{ cm}^{-1}$ were attributed to symmetric and asymmetric stretching bands of P–O(H) and PO_4^{3-} in HPO_4^{2-} , respectively. P–O(H) and PO_4^{3-} groups showed deformation absorptions at 605 and 567 cm^{-1} , respectively. The absorption peaks at 1647 and 3435 cm^{-1} were ascribed to the bending and stretching vibrations of adsorbed water –OH, respectively. In addition, the typical asymmetric stretching vibration peaks of CO_3^{2-} were observed at 1462 and 1423 cm^{-1} .²⁹ The Cs-FTIR spectrum revealed a broad band at 3469 cm^{-1} , indicating the presence of O–H and N–H stretching in the amino and hydroxyl groups. The 2920--

2875 cm^{-1} region showed a characteristic C–H stretching band. Additionally, the peak at 1660 cm^{-1} was assigned to the bending vibration of the C–H bonds of the amide I groups,^{30,31} while the 1595 cm^{-1} band corresponds to an amide II (–NH₂ bending). Other absorption peaks at 1080 and 1029 cm^{-1} were attributed to CO stretching. Analysis of the Bio-Hap/Cs beads revealed the presence of all characteristic peaks of Bio-Hap and Cs in the spectrum. In addition, a slight band shift can be observed when Cs is anchored to Bio-Hap. For example, the PO_4^{3-} peaks shifted from 1014 to 1041 cm^{-1} , possibly due to hydrogen bonding between =O and –OH of Bio-Hap and –OH of Cs. The amide II peak shifted from 1595 to 1556 cm^{-1} due to the cross-linking reaction between GA and Cs. Furthermore, an increase in the intensity of the peak at 2931 cm^{-1} , representing the characteristic C–H peak, indicated the introduction of glutaraldehyde.³²

The crystallinity evaluation of Bio-Hap, Cs, and Bio-Hap/Cs bead materials was performed through X-ray diffraction (XRD)

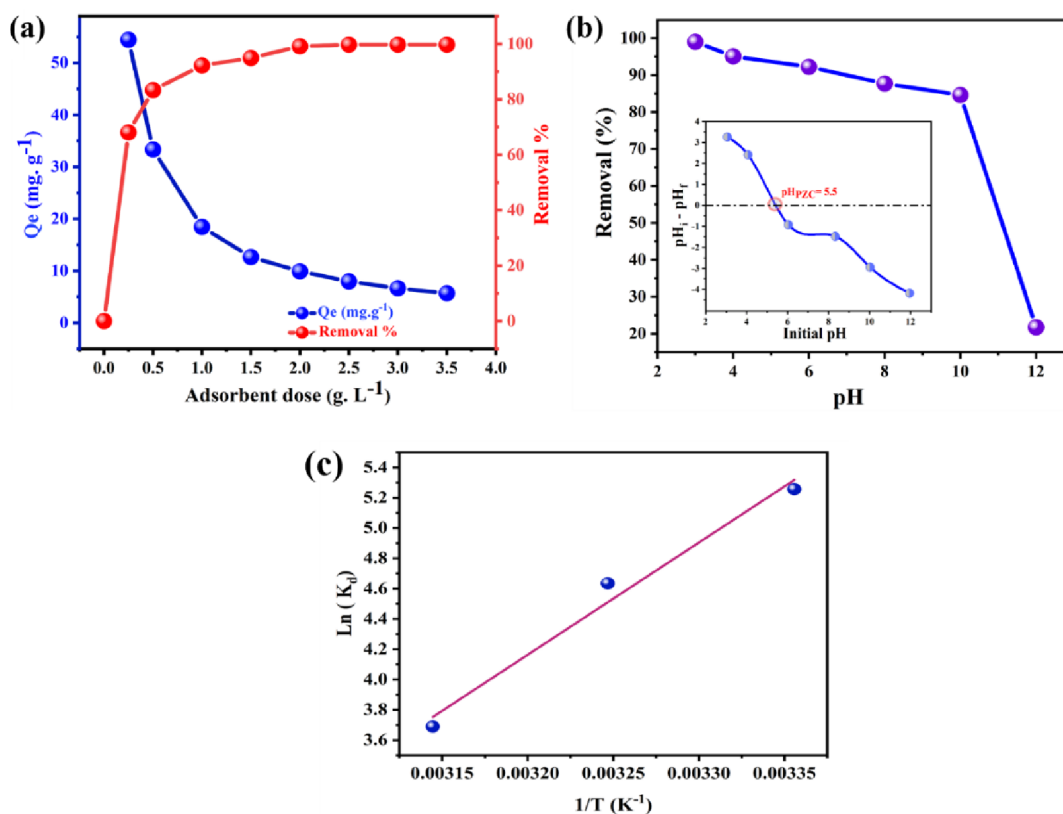


Figure 4. Analysis of adsorbent dose (a) and pH (b) effects and thermodynamic plot (c) for OG dye removal on bio-Hap/Cs beads surfaces.

Table 3. Thermodynamic Parameters for OG Dye Adsorption onto Bio-Hap/Cs Hydrogel Beads

adsorbent	ΔH (kJ mol^{-1})	ΔS ($\text{J mol}^{-1} \text{K}^{-1}$)	ΔG (kJ mol^{-1})		
			298 K	308 K	318 K
Bio-Hap/Cs beads	-61.572	-162.435	-13.017	-11.862	-9.748

analysis. Figure 2b illustrates the XRD spectrum representing these materials.³³ The peaks observed in the XRD chitosan exhibited three peaks at 13.02° , 20.11° , and 29.42° , indicating a semicrystalline structure. The XRD pattern of Bio-Hap exhibited peaks occurring at 22.84° , 25.76° , 29.12° , 32.22° , 33.98° , 39.86° , 46.72° , 49.44° , and 53.24° , corresponding to the hexagonal crystalline structure of hydroxyapatite ($\text{Ca}_{10}(\text{PO}_4)_6(\text{OH})_2$) (space group P63/m).³⁴ In the XRD diffractogram of the Bio-Hap/Cs beads, the hydroxyapatite peaks were found at 25.92° , 31.72° , 39.76° , 46.74° , 49.54° , 53.20° , and 64.09° . Additionally, a peak was detected at 13.12° , indicating the presence of intermolecular hydrogen bonding between the hydroxyl and amino functions of chitosan. This confirms the successful synthesis of the Bio-Hap/Cs beads.³⁵

Figure 3a,b illustrates the morphological structure of Bio-Hap and Cs. The SEM image of the extracted Bio-Hap reveals the presence of particles with diverse morphologies (nanoscale and microscale particles). The SEM image of the extracted chitosan clearly distinguishes the fibrillar and porous structures. Inside the SEM image of the Bio-Hap/Cs beads (Figure 3c) demonstrates that the Hap material aggregates have overlapped loosely inside the chitosan surface beads, confirming the successful development of the biobeads. After the adsorption of the dye molecules (Figure 3d), significant changes in the morphology of the Bio-Hap/Cs beads are observed.³⁶ The surface of the beads appears shiny, and the

presence of filled pores indicates the effective adsorption of the OG (organic dye) molecules on the adsorbent surface.³⁷ Furthermore, the EDS analysis of the synthesized biobeads before and after OG uptake was depicted in Figure 3e. The analysis reveals that the atomic percentages of the predominant elements in the biocomposite before the adsorption are oxygen (O) at 51.06%, carbon (C) at 41.74%, phosphorus (P) at 2.13%, calcium (Ca) at 3.80%, and nitrogen (N) at 1.27%. These elements are expected in the composition of Bio-Hap and Cs. After OG adsorption (Figure 3f), EDS elemental analysis of the Bio-Hap/Cs bead surface shows a relatively uniform distribution of each element. This indicates that the adsorbed OG molecules are evenly distributed across the surface of the beads. Moreover, a new peak attributed to the presence of sulfur (S) is observed in the EDS spectra after OG adsorption. This observation suggests that the bioadsorbent exhibits excellent performance in adsorbing OG, as the presence of sulfur indicates the successful binding of OG molecules to the surface of the beads.

3.2. Batch Adsorption. **3.2.1. pH and Adsorbent Amount Effects.** Solution pH has a significant impact on the interaction between the adsorbent and adsorbate. The variation of pH directly affects the protonation of functional groups present in the adsorbent and the ionization degree of the adsorbate.³⁸ Figure 4b shows the pH effect on OG adsorption onto Bio-Hap/Cs beads. The experiment was conducted from the pH

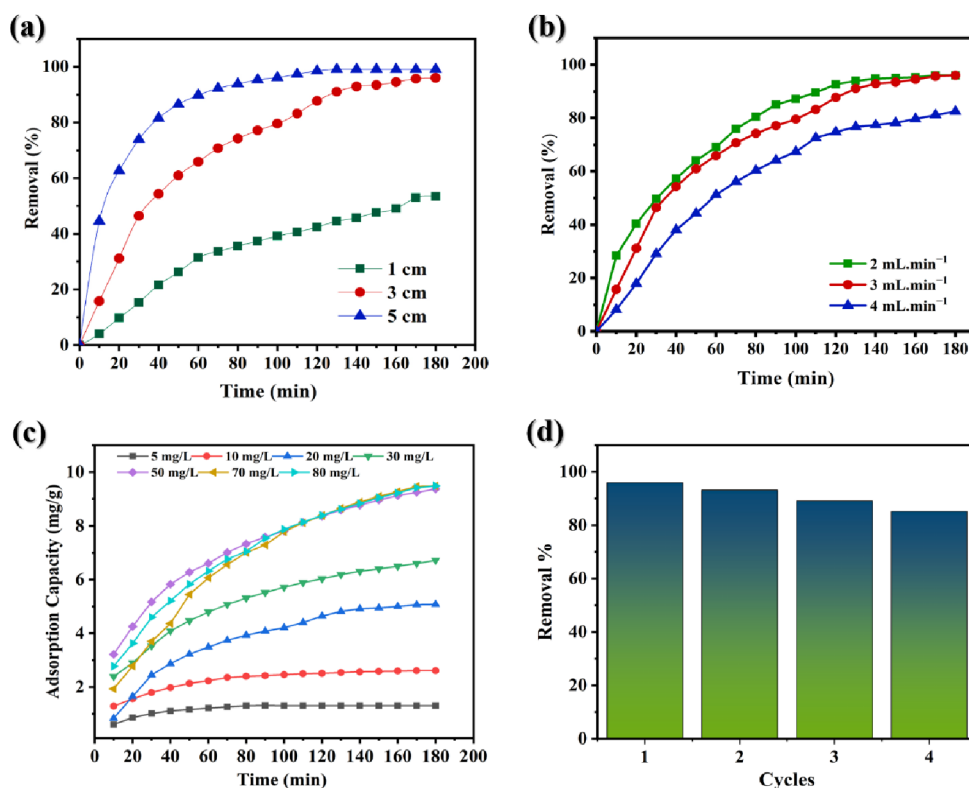


Figure 5. Analysis of bed height (a), flow rate (b), and OG dye concentration (c) effects, and the reusability of bio-Hap/Cs hydrogel beads (d).

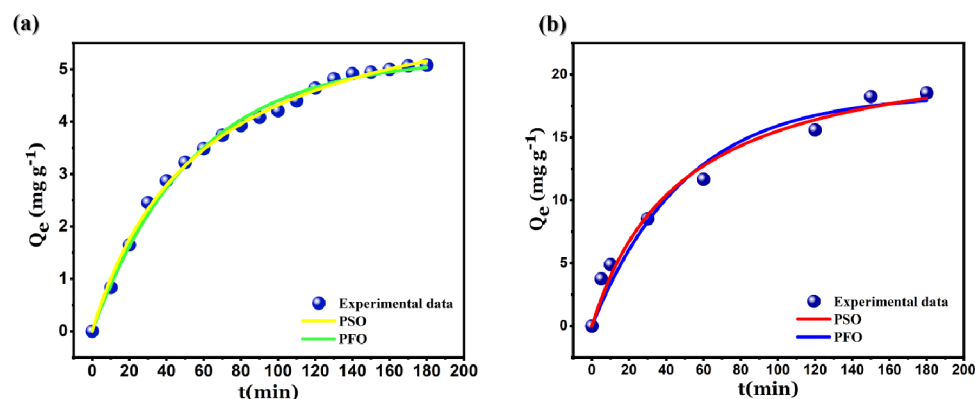


Figure 6. Nonlinear plots of PFO and PSO for OG dye adsorption onto bio-Hap/Cs beads in dynamic (a) and static (b) modes.

Table 4. Kinetic Parameters of OG Dye Removal onto Bio-Hap/Cs Beads

kinetic model	parameter	adsorbent (Bio-Hap/Cs beads)	
		batch adsorption	column adsorption
PFO model	$Q_{e,exp}$ (mg g ⁻¹)	18.46	5.098
	k_1	0.019	0.018
	$Q_{e,0.1}$	18.422	5.215
PSO model	R_2	0.971	0.995
	K_2	8.991	0.003
	$Q_{e,2}$	23.003	6.807
	R^2	0.982	0.997

range of 3 to 12. As illustrated in the figure, the adsorption percentage declined from 99% to 20% when the solution pH increased from 3 to 12, respectively. In acidic solution, the beads surface was positively charged and partially by $-NH_2$

functions in the adsorbent were protonated to NH_3^+ .³⁹ As a result, electrostatic attraction occurs between the negatively charged OG dye molecules and the positively charged surface of beads, resulting in high percentage removal. Conversely, as the pH value increases, the proportion of negative sites increases and the proportion of positive sites decreases. Based on pH_{PZC} , the surface of the adsorbent was negative above $pH = 5.5$. Thus, the electrostatic repulsion was dominating, therefore, OG dye removal was reduced. In addition, the lower adsorption of OG dye at alkaline pH was assigned to the competition of hydroxyl ions with the anionic dye.

The outcomes depicted in Figure 4a indicate that increasing the adsorbent dosage ratio from 0.25 to 3 g L⁻¹ led to an increase in OG dye adsorption from 68% to 99.71%, respectively. The adsorption capacity increased, which can be attributed to the higher number of active sites available for adsorption, resulting in an increased accessible sorption area.

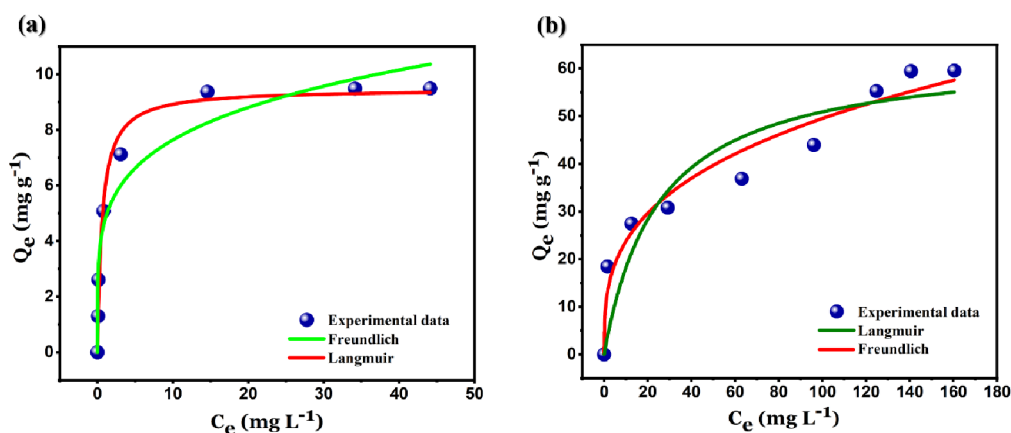


Figure 7. Nonlinear adsorption isotherm models of OG dye onto bio-Hap/Cs beads in dynamic (a) and static (b) modes.

Table 5. Nonlinear Isotherm Parameters of Langmuir and Freundlich Models for OG Adsorption onto the Bio-Hap/Cs Beads

isotherm	parameter	adsorbent (Bio-Hap/Cs)	
		batch adsorption	column adsorption
Langmuir	Q_{Exp} (mg g^{-1})	19.944	5.098
	Q_{max} (mg g^{-1})	63.572	9.472
	K_L (L mg^{-1})	0.041	1.618
	R_2	0.864	0.984
Freundlich	n_f	3.133	4.862
	K_F (mg g^{-1})	11.385	4.756
	R^2	0.962	0.940

Table 6. Comparison between the Adsorption Capacities of Several Adsorbents toward OG Dye Adsorption

adsorbent	Q_{max} (mg g^{-1})	reference
quartz sand cross-linked chitosan-glutaraldehyde	172.65	49
graft poly(<i>N</i> -vinyl-2-pyrrolidone) cross-linked chitosan beads	63.7	50
PANI@sawdust biocomposite enrobed by calcium-alginate biobeads	18.7	51
octadecylamine nanoclay	39.4	52
alumina nanoparticles	93.3	53
glutaraldehyde cross-linked Chitosan@Hydroxyapatite biocomposite	217.466	20
Bio-Hap/Cs beads (static mode)	19.944	current study
Bio-Hap/Cs beads (dynamic mode)	9.472	current study

Therefore, it can be concluded that at higher adsorbent dosage, the active sites are fully occupied by OG molecules, leading to surface saturation and higher adsorption capacity.⁴⁰

3.2.2. Thermodynamic Effect. The Gibbs free energy equations, as shown in Table 1, were used to calculate ΔG° . In addition, the thermodynamic parameters were derived from the Van't Hoff plot, as illustrated in Figure 4c and Table 3. The negative ΔG values confirm the thermodynamic spontaneity of the adsorption reactions. In addition, the negative enthalpy change ($-61.572 \text{ kJ mol}^{-1}$) suggests that the adsorption of OG dye onto the Bio-Hap/Cs beads surface is exothermic, releasing energy. Moreover, the negative ΔS value ($-162.435 \text{ kJ mol}^{-1} \text{ K}^{-1}$) indicates a reduction in randomness at the solid-solution interface during the adsorption process, implying a more ordered arrangement of molecules at the interface, which enhances dye adsorption onto the material surface.³²

In summary, the thermodynamic analysis of this research study underscores the favorable and spontaneous adsorption behavior of OG dye on the Bio-Hap/Cs beads surface. The exothermic nature of the process and the decrease in the entropy at the solid-solution interface offer valuable insights into the adsorption mechanism.

3.3. Fixed Bed Column Adsorption. **3.3.1. Effect of Bed Height.** In dynamic adsorption reactor studies, the bed height or adsorbent loading is an important monitoring factor to evaluate the performance of the adsorbent. Figure 5a shows the removal percentage of OG dye at different bed heights, with a constant flow rate of 3 mL min^{-1} and an initial concentration of 20 mg L^{-1} .⁴¹ The findings indicate that as the bed height increases, the amount of adsorbent and active surface area also increases, leading to a significant improvement in removal efficiency from 53.34% to 99.06%. From the removal percentage, it can be seen that a higher bed height or a greater amount of adsorbent in the column results in a longer bed life, and the system reaches equilibrium fast. This can be explained by the fact that a higher bed height provides more active sites for solute binding and more interaction time, reducing competition between adsorbate molecules and increasing percentage adsorption.^{42,43}

3.3.2. Effect of Flow Rate. To investigate the effect of flow rate on OG dye removal, three different flow rates of 2, 3, and 4 mL min^{-1} were used keeping the bed depth and inlet OG dye concentration remained constant at 3 cm and 20 mg L^{-1} at $\text{pH} = 6$. Figure 5b presents the curve illustrating the effect of various flow rates on OG dye removal.^{43,44} The results demonstrated that a decrease in the flow rate led to an increase in the percentage of OG dye removal and the time taken to reach saturation. At a lower flow rate, the OG dye had more time to contact the Bio-Hap/Cs beads' sorption site, resulting in a higher removal of OG molecules in the column system. Conversely, at a higher flow rate, the adsorption capacity was lower, as the lower residence time of the solute results in less diffusion into the pores of the adsorbent. Overall, the study suggests that achieving higher removal efficiencies requires a longer contact time between the adsorbent and solute, which can be achieved by lowering the flow rate.⁴⁵

3.3.3. Effect of Influent OG Dye Concentration. In this study, the effect of initial OG dye concentration on the adsorption effectiveness of Bio-Hap/Cs beads was explored and is depicted in Figure 5c. The findings revealed a significant decline in the percentage removal of OG dye from 98.66% to 44.85% when the initial OG dye concentration increased from

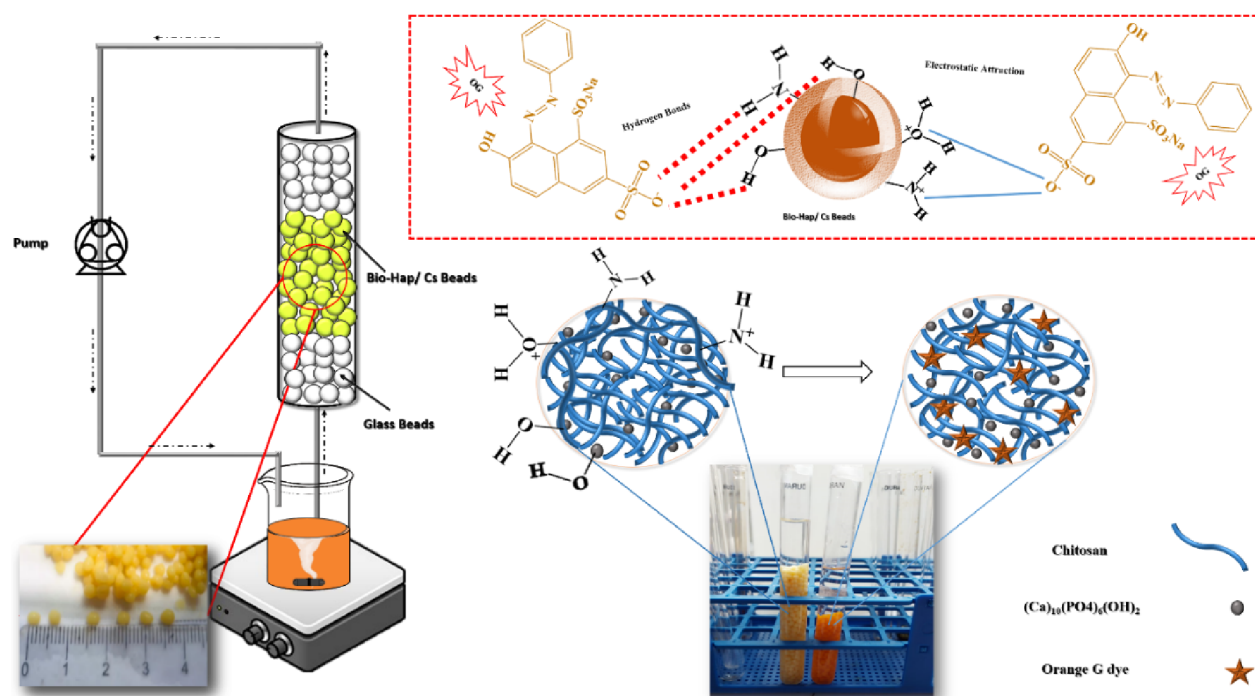


Figure 8. Proposed adsorption mechanism for OG dye on bio-Hap/Cs beads in static and dynamic modes.

Table 7. Experimental Levels for OG Adsorption on Bio-Hap/Cs Hydrogel Beads and CCD Matrix

run	coded values			real values			removal efficiency (%)
	X_{AD}	X_{OG}	X_{CT}	adsorbent dose (g/l)	concentration of OG (mg/L)	contact time (min)	
1	-1	-1	-1	10	15	120	39.55
2	1	-1	-1	20	15	120	83.45
3	-1	1	-1	10	25	120	33.33
4	1	1	-1	20	25	120	70.73
5	-1	-1	1	10	15	180	48.02
6	1	-1	1	20	15	180	95.48
7	-1	1	1	10	25	180	39.55
8	1	1	1	20	25	180	75.71
9	-r	0	0	6.59	20	150	41.24
10	+r	0	0	23.41	20	150	94.63
11	0	-r	0	15	11.59	150	96.23
12	0	+r	0	15	28.41	150	61.06
13	0	0	-r	15	20	99.54	69.04
14	0	0	+r	15	20	200.45	85.45
15	0	0	0	15	20	150	81.36
16	0	0	0	15	20	150	82.02
17	0	0	0	15	20	150	82.11
18	0	0	0	15	20	150	81.09
19	0	0	0	15	20	150	81.67
20	0	0	0	15	20	150	81.31

5 to 80 mg L⁻¹.⁴⁶ However, the quantity of OG dye adsorbed by the Bio-Hap/Cs beads increased from 1.31 to 9.49 mg g⁻¹. This can be attributed to the fact that as the inlet concentration of OG dye increases, the interaction time between OG molecules and the surface Bio-Hap/Cs beads increases and the number of vacant active sites for biosorption also increases. These findings have significant implications for the practical application of the Bio-Hap/Cs beads adsorbent in wastewater treatment as they suggest that the adsorbent is capable of effectively removing OG dye from wastewater at various initial concentrations.

3.3.4. Regeneration. The potential for recycling and regenerating an adsorption column holds significant promise in extending its operational lifespan and mitigating the treatment costs associated with dye wastewater. In practical applications, the recovery and stability of the sorbent material are crucial factors to consider. Therefore, the reusability of the dye-loaded Bio-Hap/Cs beads was evaluated using NaOH solution (0.1 M), and the adsorptive activity of the beads was examined over four successive adsorption/desorption cycles, as depicted in Figure 5d. The figure clearly revealed that the adsorption rate remained high, with an average retention of approximately 95.19% maintained throughout the four cycles.

Table 8. Analysis of Variance (ANOVA) for OG Removal

terms	coefficient	F-value	p-value (%)
model		10.74	0.0005
constant	82.03	65.23	
X ₁	18.65	11.37	<0.0001
X ₂	-7.79	3.54	0.0071
X ₃	4.34	0.54	0.0895
X ₁₋₁	-7.67	11.64	0.0066
X ₂₋₂	-3.88	2.98	0.1149
X ₃₋₃	-4.38	3.79	0.0801
X ₁₋₂	-2.23	0.01	0.4778
X ₁₋₃	0.29	0.15	0.9253
X ₂₋₃	-1.16	11.64	0.7081
lack of fit		862.95	<0.0001
R ²	0.906		
R ² _{Adj}	0.821		
R ² _{Pre}	0.2916		

Consequently, the results of the reusability assessment underscore the significant potential of the Bio-Hap/Cs beads as a cost-effective adsorbent.

3.4. Kinetic Study. The effect of contact time on dye adsorption onto Bio-Hap/Cs beads is shown in Figure 6. As can be seen, the adsorption capacity increased as the contact time increased until equilibrium was reached at 180 min. The rapid adsorption rate observed in the initial minutes was due to the availability of active sites on the beads surface.⁴⁷ However, the aggregation of dye molecules within the beads may hinder the diffusion of adsorbed molecules, leading to a slower adsorption rate. To investigate the appropriate model describing the adsorption of OG dye, kinetic adsorption was evaluated by applying PFO and PSO models for both batch and recirculating column processes. The fitted curves Figure 6a,b and fitting parameters (Table 4) show that the pseudo-second-order model describes well OG dye adsorption on Bio-Hap/Cs hydrogel beads rather than the pseudo-first-order kinetic model using both adsorption modes. These results declare that the rate-determining adsorption step could be chemisorption involving valence forces through the exchange or sharing of electrons between the adsorbate and adsorbent.⁴⁸

3.5. Adsorption Isotherm. The aim of this study was to explore the adsorption isotherms of OG dye on Bio-Hap/Cs beads in order to determine the maximum loading capacity and to investigate the interaction between the adsorbent surface sites and adsorbate molecules. To achieve this, both batch and recirculating column processes were used, and the experimental equilibrium data were plotted using the Langmuir and Freundlich isotherm models, Figure 7ab. The results showed that the adsorption capacity increased with an increasing dye concentration, indicating that the available binding sites became saturated as more dye was added to the aqueous solution. In the static mode, the equilibrium data for OG dye adsorption onto Bio-Hap/Cs beads best fit the Freundlich model, which describes a heterogeneous surface system. In this system, stronger binding sites are occupied first, followed by a decrease in the degree of occupation with binding strength. In contrast, the Langmuir adsorption isotherm better described the equilibrium data obtained from the recirculating column process, which assumes monolayer adsorption and a finite number of homogeneous adsorption sites. The coefficient of correlation for both the Langmuir and Freundlich adsorption isotherms was determined by applying the experimental

adsorption equilibrium results, and the values were reported in Table 5. The results suggest that the Freundlich model provided a good fit for the equilibrium data obtained in the static mode, while the Langmuir adsorption isotherm was more appropriate for the recirculating column process. The results from this study could be valuable in the development of efficient and effective methods for removing OG dye from aqueous solutions.

3.6. Comparison. To evaluate the adsorption efficacy of Bio-Hap/Cs beads toward the OG dye, a comparative analysis with other sorbents previously documented in the scientific literature was carried out, as summarized in Table 6. The experimental outcomes illustrate the notable superiority of the Bio-Hap/Cs beads in terms of its sorption efficacy, surpassing the performance exhibited by alternative sorbents. The higher adsorption capacity of the Bio-Hap/Cs beads can be ascribed to its distinctive surface characteristics, encompassing a combination of both organic (chitosan) and inorganic (calcium phosphate) functional groups. Overall, the Bio-Hap/Cs beads emerge as a highly promising adsorbent for the selective removal of anionic dyes from aqueous solutions.

3.7. Mechanism. In order to enhance our comprehension of the sorption mechanism, the biobeads Bio-Hap/Cs underwent characterization using SEM/EDS (Figure 2) and FTIR analysis (Figure 2a) subsequent to the adsorption of dye. The FTIR spectral data exhibited the presence of several prominent functional groups on the surface of Bio-Hap/Cs beads, encompassing organic (chitosan chain) and inorganic (calcium phosphate) hydroxyl and primary–secondary amine groups. After the adsorption of OG dye molecules, notable shifts in the position of bands located at 1662 and 1556 cm⁻¹ were observed in the FTIR spectrum (Figure 2a), indicating the interaction between OG dye molecules containing sulfonate groups and the binding sites of the biobeads via hydrogen bonding and electrostatic forces. The disappearance of the adsorption band at 3340 cm⁻¹ (associated with the stretching vibration of OH and NH₂) suggests saturation of binding sites with OG dye molecules. Furthermore, a new adsorption band appeared at 1230 cm⁻¹, attributed to S=O stretching, further confirming the successful adsorption of OG dye. The bands within the range of 1500 to 1700 cm⁻¹, corresponding to the overlapping stretching vibrations of amines and the characteristic aromatic skeletal structure, were assigned to the effective adsorption of OG dye by the Bio-Hap/Cs beads. The EDS spectrum of the biocomposite loaded with OG dye exhibited a new peak corresponding to elemental sulfur (S), providing additional evidence supporting the excellent performance of the bioadsorbent. A visual representation depicting the potential interactions between OG molecules and the surface of Bio-Hap/Cs beads is presented in Figure 8.

3.8. Optimization of Adsorption Process. In this part of the study, the primary objective is to optimize the adsorption process of OG dye using Bio-Hap/Cs beads by applying the response surface methodology (RSM) approach (Table 7). Several parameters were systematically investigated, analyzing both their individual and interactive effects on the adsorption performance of OG dye. The mathematical model obtained was rigorously validated using ANOVA (analysis of variance). The ANOVA results (Table 8) demonstrate the statistical significance of the proposed model, with *p*-values below 5%. Furthermore, the correlation coefficient (*R*²) and adjusted correlation coefficient (*R*²_{adj}) were determined to be 0.906 and

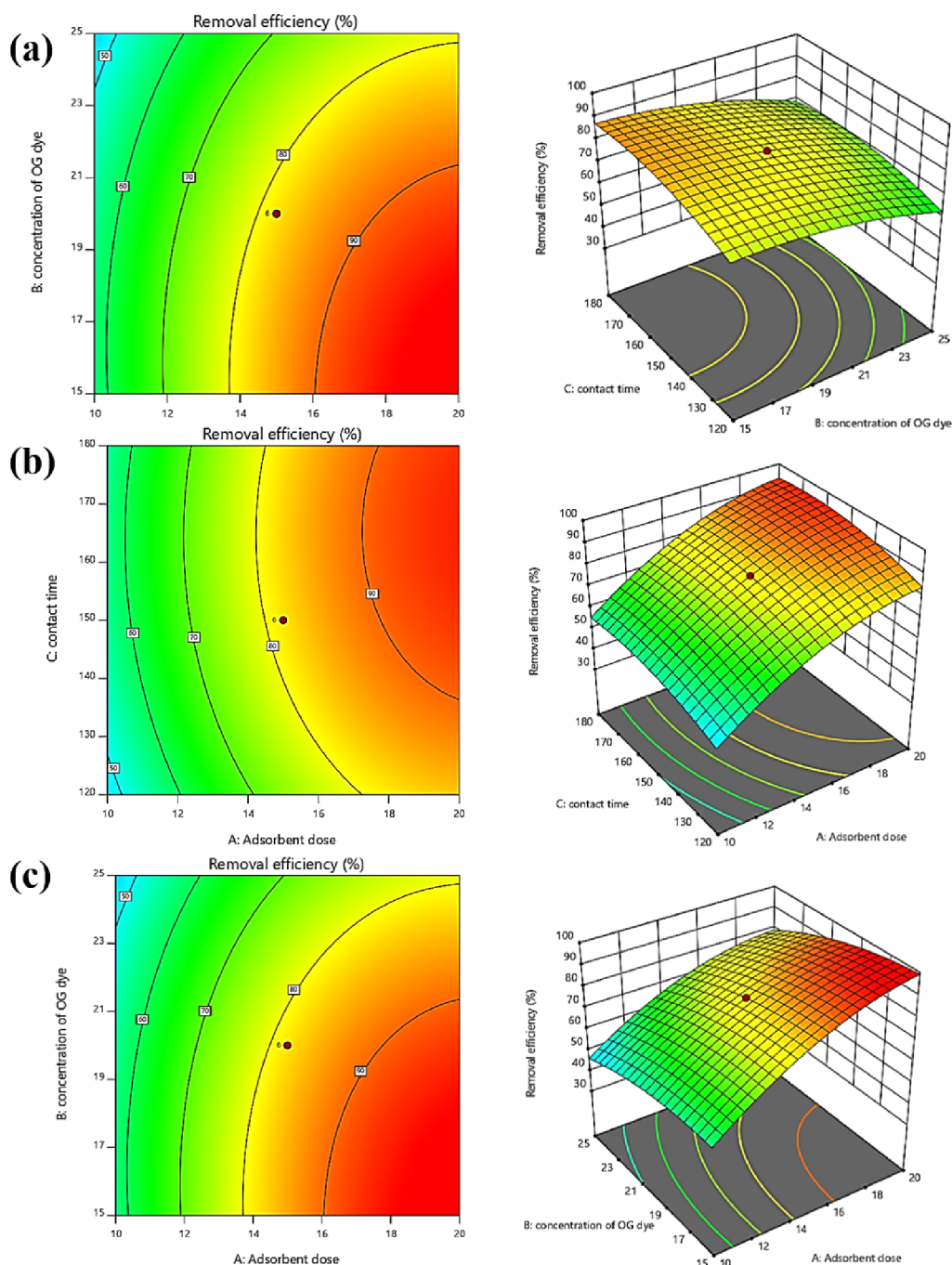


Figure 9. 2D–3D surface plots of the effect of the interaction between concentration of OG and adsorbent dose (a), contact time and concentration of OG (b), and contact time and adsorbent dose (c) on removal of OG (%).

0.822, respectively. These findings support a robust agreement between the predicted and experimental results. The quadratic polynomial model can be expressed as follows:

$$\begin{aligned} \text{Removal\%} = & 82.03 + 18.65X_{\text{AD}} - 7.79X_{\text{OG}} + 4.34X_{\text{CT}} \\ & - 7.67X_{\text{AD-AD}}^2 - 3.88X_{\text{OG-OG}}^2 \\ & - 4.38X_{\text{CT-CT}}^2 - 2.23X_{\text{AD-OG}} \\ & + 0.29X_{\text{AD-CT}} - 1.16X_{\text{OG-CT}} \end{aligned}$$

Response surface design (3D) used the second-order quadratic equation to determine optimal values for the selected factors. These 3D models effectively showed how

different factors and their interactions affected the adsorption process.

Figure 9c illustrates the interdependent relationship between the adsorbent material dose of (Bio-Hap/Cs beads) and the initial concentration of OG. It was observed that the removal percentage of OG dye showed an increasing trend as the mass of Bio-Hap/Cs beads increased from 7 to 23 mg, accompanied by a decrease in dye concentration from 28 to 12 ppm. This behavior suggests that optimal adsorption performance is achieved when a larger number of active adsorption sites are available.

The binary interaction effect between the contact time and initial concentration of OG is indicated in Figure 9a. Notably,

the percentage removal of OG was relatively low at higher adsorbate concentrations, a phenomenon probably due to the reduced ratio of accessible adsorption sites to solute concentration.

Figure 9b shows the interaction effect of the adsorbent dose and the contact time. As can be seen from the 3D graph, a contact time, ranging from 100 to 200 min, leads to improved dye adsorption efficiency. Thus, by using a large amount of adsorbent and a sufficient contact time, the saturation of the active adsorption sites can be promoted.

As a result of these findings, the optimal removal of OG dye was determined to be 93%, achievable under the following conditions: 20 mg of Bio-Hap/Cs beads, a OG concentration of 20 ppm, and a contact time of 150 min.

4. CONCLUSION

In this research, we introduced a novel approach for the synthesis of biobeads using fish scale extracted Bio-Hap powder encapsulated by chitosan cross-linking. The resulting beads possess a special cross-linked network structure and abundant functional groups, which exhibit outstanding adsorption performance toward Orange G (OG) dye in batch and recirculating column processes. Our findings indicate that the kinetic behavior of Bio-Hap/Cs beads can be effectively described by the pseudo-second-order model in both batch and recirculating column methods. In the fixed-bed process, higher bed height and low flow rate were amenable factors for wastewater treatment with extremely low OG dye concentration. Without a doubt, this innovative approach of utilizing fish-scale-extracted Bio-Hap proves to be a highly efficient method for wastewater treatment, particularly in industrial settings. Overall, the obtained composite beads exhibit excellent reusability properties, as they can be easily recovered from water and reused for several cycles, which presents an economically advantageous aspect of the adsorption process.

AUTHOR INFORMATION

Corresponding Authors

Bouthayna Kjidaa – Team of Biotechnology, Materials and Environment, Faculty of Sciences, Ibn Zohr University, Agadir 80000, Morocco; orcid.org/0000-0003-0720-1924; Email: bouthayna.kjidaa@edu.uiz.ac.ma

Rachid Mamouni – Team of Biotechnology, Materials and Environment, Faculty of Sciences, Ibn Zohr University, Agadir 80000, Morocco; Email: r.mamouni@uiz.ac.ma

Authors

Zaineb Mchich – Team of Biotechnology, Materials and Environment, Faculty of Sciences, Ibn Zohr University, Agadir 80000, Morocco

Khalid Aziz – Team of Biotechnology, Materials and Environment, Faculty of Sciences, Ibn Zohr University, Agadir 80000, Morocco

Nabil Saffaj – Team of Biotechnology, Materials and Environment, Faculty of Sciences, Ibn Zohr University, Agadir 80000, Morocco

Taoufiq Saffaj – Laboratory of Applied Organic Chemistry, Faculty of Sciences and Techniques of Fez, University Sidi Mohamed Ben Abdellah, Fez 30000, Morocco

Complete contact information is available at:

<https://pubs.acs.org/10.1021/acsomega.3c10054>

Notes

The authors declare no competing financial interest.

ACKNOWLEDGMENTS

No external funding agency was involved in this work. The authors would like to express their gratitude to the Faculty of Sciences at University Ibn Zohr, Agadir, particularly the Biotechnologies, Materials, and Environment team, for providing instrumental facilities to analyze the samples and for their consistent support throughout the research process.

REFERENCES

- (1) Chen, J.; Xiong, Y.; Duan, M.; Li, X.; Li, J.; Fang, S.; Qin, S.; Zhang, R. Insight into the Synergistic Effect of Adsorption–Photocatalysis for the Removal of Organic Dye Pollutants by Cr-Doped ZnO. *Langmuir* **2020**, *36* (2), 520–533.
- (2) Mittal, H.; Babu, R.; Dabbawala, A. A.; Alhassan, S. M. Low-Temperature Synthesis of Magnetic Carbonaceous Materials Coated with Nanosilica for Rapid Adsorption of Methylene Blue. *ACS Omega* **2020**, *5* (11), 6100–6112.
- (3) Senguttuvan, S.; Janaki, V.; Senthilkumar, P.; Kamala-Kannan, S. Polypyrrole/Zeolite Composite – A Nano-adsorbent for Reactive Dyes Removal from Synthetic Solution. *Chemosphere* **2022**, *287*, 132164.
- (4) El Gaayda, J.; Titchou, F. E.; Barra, I.; Karmal, I.; Afanga, H.; Zazou, H.; Yap, P.-S.; Abidin, Z. Z.; Hamdani, M.; Akbour, R. A. Optimization of Turbidity and Dye Removal from Synthetic Wastewater Using Response Surface Methodology: Effectiveness of Moringa Oleifera Seed Powder as a Green Coagulant. *J. Environ. Chem. Eng.* **2022**, *10* (1), 106988.
- (5) Akhsassi, B.; Naciri, Y.; Bouddouch, A.; Bakiz, B.; Taoufiq, A.; Villain, S.; Favotto, C.; Valmalette, J.-C.; Gavarri, J.-R.; Benhachemi, A. Facile Novel Acid Coprecipitation Synthesis of BiPO₄ Polymorphs: Enhanced Photocatalytic Degradation of the Antibiotic AMX and the Dyes RhB, MB and MO. *Opt. Mater.* **2023**, *137*, 113575.
- (6) Liu, H.; Zhang, J.; Lu, M.; Liang, L.; Zhang, H.; Wei, J. Biosynthesis Based Membrane Filtration Coupled with Iron Nanoparticles Reduction Process in Removal of Dyes. *Chem. Eng. J.* **2020**, *387*, 124202.
- (7) Amjlef, A.; Farsad, S.; Ait El Fakir, A.; El Asri, A.; El Issami, S.; Et-Taleb, S.; El Alem, N. Polyaniline-Encapsulated Quartz Sand as an Adsorbent Composite for Orange G Dye Removal from Aqueous Solution: Experimental and Computational Study. *Ceram. Int.* **2023**, *49* (9), 14120–14134.
- (8) Aziz, K.; Aziz, F.; Mamouni, R.; Aziz, L.; Anfar, Z.; Azrrar, A.; Kjidaa, B.; Saffaj, N.; Laknifli, A. High Thiabendazole Fungicide Uptake Using *Cellana Tramoserica* Shells Modified by Copper: Characterization, Adsorption Mechanism, and Optimization Using CCD-RSM Approach. *Environ. Sci. Pollut. Res.* **2022**, *29* (57), 86020–86035.
- (9) Mashabi, R. A.; Khan, Z. A.; Elwakeel, K. Z. Chitosan- or Glycidyl Methacrylate-Based Adsorbents for the Removal of Dyes from Aqueous Solutions: A Review. *Mater. Adv.* **2022**, *3* (14), 5645–5671.
- (10) Xiong, Y.; Zhang, C.; Duan, M.; Chen, J.; Fang, S.; Li, J.; Shi, P.; Ren, J.; Wan, H. Insight into Organic Pollutant Adsorption Characteristics on a G-C₃N₄ Surface by Attenuated Total Reflection Spectroscopy and Molecular Dynamics Simulation. *Langmuir* **2021**, *37* (25), 7655–7667.
- (11) Baraka, N. E.; Saffaj, N.; Mamouni, R.; Laknifli, A.; Younsi, S. A.; Albizane, A.; El Haddad, M. Elaboration of a New Flat Membrane Support from Moroccan Clay. *Desalin. Water Treat.* **2014**, *52* (7–9), 1357–1361.
- (12) El Qacimi, N.; El Baraka, N.; Saffaj, N.; Mamouni, R.; Laknifli, A.; Alami Younsi, S.; Faouzi, A.; Zidouh, H. Preparation and Characterization of Flat Membrane Support Based on Sahara Moroccan Clay: Application to the Filtration of Textile Effluents. *Desalin. Water Treat.* **2019**, *143*, 111–117.

- (13) Ahmadian, M.; Derakhshankhah, H.; Jaymand, M. Biosorptive Removal of Organic Dyes Using Natural Gums-Based Materials: A Comprehensive Review. *J. Ind. Eng. Chem.* **2023**, *124*, 102–131.
- (14) Moosavi, S.; Lai, C. W.; Gan, S.; Zamiri, G.; Akbarzadeh Pivezhzani, O.; Johan, M. R. Application of Efficient Magnetic Particles and Activated Carbon for Dye Removal from Wastewater. *ACS Omega* **2020**, *5* (33), 20684–20697.
- (15) Nordin, A. H.; Ngadi, N.; Nordin, M. L.; Noralidin, N. A.; Nabgan, W.; Osman, A. Y.; Shaari, R. Spent Tea Waste Extract as a Green Modifying Agent of Chitosan for Aspirin Adsorption: Fixed-Bed Column, Modeling and Toxicity Studies. *Int. J. Biol. Macromol.* **2023**, *253*, 126501.
- (16) Chen, C.; He, E.; Jia, W.; Xia, S.; Yu, L. Preparation of Magnetic Sodium Alginate/Sodium Carboxymethylcellulose Interpenetrating Network Gel Spheres and Use in Superefficient Adsorption of Direct Dyes in Water. *J. Biol. Macromol.* **2023**, *253*, 126985.
- (17) Arni, L. A.; Hapiz, A.; Abdulhameed, A. S.; Khadiran, T.; AlOthman, Z. A.; Wilson, L. D.; Jawad, A. H. Design of Separable Magnetic Chitosan Grafted-Benzaldehyde for Azo Dye Removal via a Response Surface Methodology: Characterization and Adsorption Mechanism. *Int. J. Biol. Macromol.* **2023**, *242*, 125086.
- (18) Aziz, K.; Mamouni, R.; Azrar, A.; Kjidaa, B.; Saffaj, N.; Aziz, F. Enhanced Biosorption of Bisphenol A from Wastewater Using Hydroxyapatite Elaborated from Fish Scales and Camel Bone Meal: A RSM@BBD Optimization Approach. *Ceram. Int.* **2022**, *48* (11), 15811–15823.
- (19) Umesh, M.; Choudhury, D. D.; Shanmugam, S.; Ganesan, S.; Alsehli, M.; Elfasakhany, A.; Pugazhendhi, A. Eggshells Biowaste for Hydroxyapatite Green Synthesis Using Extract Piper Betel Leaf - Evaluation of Antibacterial and Antibiofilm Activity. *Environ. Res.* **2021**, *200*, 111493.
- (20) Kjidaa, B.; Mamouni, R.; Aziz, K.; Saffaj, T.; Adraoui, I.; Mchich, Z.; Saffaj, N. Green Synthesis of a Biomaterial Composite Based on Fish Scales for Anionic Dye Removal: Characterization and Optimization by RSM@BBD Approach. *Water Air Soil Pollut* **2023**, *234* (6), 352.
- (21) Heidari, F.; Razavi, M.; Bahrololoom, M. E.; Tahriri, M.; Rasoulianboroujeni, M.; Koturi, H.; Tayebi, L. Preparation of Natural Chitosan from Shrimp Shell with Different Deacetylation Degree. *Mater. Res. Innov* **2018**, *22* (3), 177–181.
- (22) Abdelaziz, M. A.; Owda, M. E.; Abouzeid, R. E.; Alaysuy, O.; Mohamed, E. I. Kinetics, Isotherms, and Mechanism of Removing Cationic and Anionic Dyes from Aqueous Solutions Using Chitosan/Magnetite/Silver Nanoparticles. *Water, Air, Soil Pollut* **2023**, *225*, 1462–1475.
- (23) Ho, Y. S.; McKay, G. Pseudo-Second Order Model for Sorption Processes. *Process Biochem.* **1999**, *34* (5), 451–465.
- (24) Jain, S. N.; Shaikh, Z.; Mane, V. S.; Vishnoi, S.; Mawal, V. N.; Patel, O. R.; Bhandari, P. S.; Gaikwad, M. S. Nonlinear Regression Approach for Acid Dye Remediation Using Activated Adsorbent: Kinetic, Isotherm, Thermodynamic and Reusability Studies. *Microchem. J.* **2019**, *148*, 605–615.
- (25) Ncibi, M. C. Applicability of Some Statistical Tools to Predict Optimum Adsorption Isotherm after Linear and Non-Linear Regression Analysis. *J. Hazard. Mater.* **2008**, *153* (1–2), 207–212.
- (26) Ng, J. C. Y.; Cheung, W. H.; McKay, G. Equilibrium Studies for the Sorption of Lead from Effluents Using Chitosan. *Chemosphere* **2003**, *52* (6), 1021–1030.
- (27) Senturk, H. B.; Ozdes, D.; Gundogdu, A.; Duran, C.; Soylak, M. Removal of Phenol from Aqueous Solutions by Adsorption onto Organomodified Tirebolu Bentonite: Equilibrium, Kinetic and Thermodynamic Study. *J. Hazard. Mater.* **2009**, *172* (1), 353–362.
- (28) Kou, T.; Wang, Y.; Zhang, C.; Sun, J.; Zhang, Z. Adsorption Behavior of Methyl Orange onto Nanoporous Core–Shell Cu@Cu₂O Nanocomposite. *Chem. Eng. J.* **2013**, *223*, 76–83.
- (29) Shi, P.; Liu, M.; Fan, F.; Yu, C.; Lu, W.; Du, M. Characterization of Natural Hydroxyapatite Originated from Fish Bone and Its Biocompatibility with Osteoblasts. *Mater. Sci. Eng., C* **2018**, *90*, 706–712.
- (30) Chatterjee, S.; Gupta, A.; Mohanta, T.; Mitra, R.; Samanta, D.; Mandal, A. B.; Majumder, M.; Rawat, R.; Singha, N. R. Scalable Synthesis of Hide Substance–Chitosan–Hydroxyapatite: Novel Biocomposite from Industrial Wastes and Its Efficiency in Dye Removal. *ACS Omega* **2018**, *3* (9), 11486–11496.
- (31) Sirajudheen, P.; Karthikeyan, P.; Ramkumar, K.; Meenakshi, S. Effective Removal of Organic Pollutants by Adsorption onto Chitosan Supported Graphene Oxide-Hydroxyapatite Composite: A Novel Reusable Adsorbent. *J. Mol. Liq.* **2020**, *318*, 114200.
- (32) Rastgordani, M.; Zolgharnein, J. Simultaneous Determination and Optimization of Titan Yellow and Reactive Blue 4 Dyes Removal Using Chitosan@hydroxyapatite Nanocomposites. *J. Polym. Environ.* **2021**, *29* (6), 1789–1807.
- (33) Jing, X.; Mi, H.-Y.; Turng, L.-S. Comparison between PCL/Hydroxyapatite (HA) and PCL/Halloysite Nanotube (HNT) Composite Scaffolds Prepared by Co-Extrusion and Gas Foaming. *Mater. Sci. Eng., C* **2017**, *72*, 53–61.
- (34) Sadeghianmaryan, A.; Naghieh, S.; Yazdanpanah, Z.; Alizadeh Sardroud, H.; Sharma, N. K.; Wilson, L. D.; Chen, X. Fabrication of Chitosan/Alginate/Hydroxyapatite Hybrid Scaffolds Using 3D Printing and Impregnating Techniques for Potential Cartilage Regeneration. *Int. J. Biol. Macromol.* **2022**, *204*, 62–75.
- (35) Hernández-Cocoletzi, H.; Salinas, R. A.; Aguila-Almanza, E.; Rubio-Rosas, E.; Chai, W. S.; Chew, K. W.; Mariscal-Hernández, C.; Show, P. L. Natural Hydroxyapatite from Fishbone Waste for the Rapid Adsorption of Heavy Metals of Aqueous Effluent. *Environ. Technol. Innovation* **2020**, *20*, 101109.
- (36) Wan Ngah, W. S.; Endud, C. S.; Mayanar, R. Removal of Copper(II) Ions from Aqueous Solution onto Chitosan and Cross-Linked Chitosan Beads. *React. Funct. Polym* **2002**, *50* (2), 181–190.
- (37) Li, L.; Iqbal, J.; Zhu, Y.; Zhang, P.; Chen, W.; Bhatnagar, A.; Du, Y. Chitosan/Ag-Hydroxyapatite Nanocomposite Beads as a Potential Adsorbent for the Efficient Removal of Toxic Aquatic Pollutants. *Int. J. Biol. Macromol.* **2018**, *120*, 1752–1759.
- (38) Khan, M. I.; Shanableh, A.; Elboughdiri, N.; Lashari, M. H.; Manzoor, S.; Shahida, S.; Farooq, N.; Bouazzi, Y.; Rejeb, S.; Elleuch, Z.; Kriaa, K.; Ur Rehman, A. Adsorption of Methyl Orange from an Aqueous Solution onto a BPPO-Based Anion Exchange Membrane. *ACS Omega* **2022**, *7* (30), 26788–26799.
- (39) Munagapati, V. S.; Yarramuthi, V.; Kim, D.-S. Methyl Orange Removal from Aqueous Solution Using Goethite, Chitosan Beads and Goethite Impregnated with Chitosan Beads. *J. Mol. Liq.* **2017**, *240*, 329–339.
- (40) Mallakpour, S.; Behranvand, V.; Mallakpour, F. Adsorptive Performance of Alginate/Carbon Nanotube-Carbon Dot-Magnesium Fluorohydroxyapatite Hydrogel for Methylene Blue-Contaminated Water. *J. Environ. Chem. Eng.* **2021**, *9* (2), 105170.
- (41) Das, L.; Sengupta, S.; Das, P.; Bhowal, A.; Bhattacharjee, C. Experimental and Numerical Modeling on Dye Adsorption Using Pyrolyzed Mesoporous Biochar in Batch and Fixed-Bed Column Reactor: Isotherm, Thermodynamics, Mass Transfer, Kinetic Analysis. *Surf. Interfaces* **2021**, *23*, 100985.
- (42) Biswas, S.; Mohapatra, S. S.; Kumari, U.; Meikap, B. C.; Sen, T. K. Batch and Continuous Closed Circuit Semi-Fluidized Bed Operation: Removal of MB Dye Using Sugarcane Bagasse Biochar and Alginate Composite Adsorbents. *J. Environ. Chem. Eng.* **2020**, *8* (1), 103637.
- (43) Bakka, A.; Mamouni, R.; Saffaj, N.; Laknifli, A.; Aziz, K.; Roudani, A. Removal of Bifenthrin Pesticide from Aqueous Solutions by Treated Patellidae Shells Using a New Fixed Bed Column Filtration Technique. *Process Saf. Environ. Prot* **2020**, *143*, 55–65.
- (44) Jain, M.; Garg, V. K.; Kadirvelu, K. Cadmium(II) Sorption and Desorption in a Fixed Bed Column Using Sunflower Waste Carbon Calcium–Alginate Beads. *Bioresour. Technol.* **2013**, *129*, 242–248.
- (45) Murambasvina, G.; Mahamadi, C. Effective Fluoride Adsorption Using Water Hyacinth Beads Doped with Hydroxyl

Oxides of Aluminium and Iron. *Groundw. Sustain. Dev.* **2020**, *10*, 100302.

(46) Aziz, K.; El Achaby, M.; Mamouni, R.; Saffaj, N.; Aziz, F. A Novel Hydrogel Beads Based Copper-Doped Cerastoderma Edule shells@Alginate Biocomposite for Highly Fungicide Sorption from Aqueous Medium. *Chemosphere* **2023**, *311*, 136932.

(47) Xu, S.; Jin, Y.; Li, R.; Shan, M.; Zhang, Y. Amidoxime Modified Polymers of Intrinsic Microporosity/Alginate Composite Hydrogel Beads for Efficient Adsorption of Cationic Dyes from Aqueous Solution. *J. Colloid. Interface. Sci.* **2022**, *607*, 890–899.

(48) Pour, Z. S.; Ghaemy, M. Removal of Dyes and Heavy Metal Ions from Water by Magnetic Hydrogel Beads Based on Poly (Vinyl Alcohol)/Carboxymethyl Starch-g-Poly (Vinyl Imidazole). *RSC Adv.* **2015**, *5* (79), 64106–64118.

(49) Amjlef, A.; Farsad, S.; Chaoui, A.; Ben Hamou, A.; Ezzahery, M.; Et-Taleb, S.; El Alem, N. Effective Adsorption of Orange G Dye Using Chitosan Cross-Linked by Glutaraldehyde and Reinforced with Quartz Sand. *Int. J. Biol. Macromol.* **2023**, *239*, 124373.

(50) Sutirman, Z. A.; Sanagi, M. M.; Abd Karim, K. J.; Abu Naim, A.; Wan Ibrahim, W. A. Enhanced Removal of Orange G from Aqueous Solutions by Modified Chitosan Beads: Performance and Mechanism. *Int. J. Biol. Macromol.* **2019**, *133*, 1260–1267.

(51) Imgharn, A.; Aarab, N.; Hsini, A.; Naciri, Y.; Elhoudi, M.; Haki, M. A.; Laabd, M.; Lakhmiri, R.; Albourine, A. Application of Calcium Alginate-PANI@sawdust Wood Hydrogel Bio-Beads for the Removal of Orange G Dye from Aqueous Solution. *Environ. Sci. Pollut. Res.* **2022**, *29* (40), 60259–60268.

(52) Salam, M. A.; Kosa, S. A.; Al-Beladi, A. A. Application of Nanoclay for the Adsorptive Removal of Orange G Dye from Aqueous Solution. *J. Mol. Liq.* **2017**, *241*, 469–477.

(53) Banerjee, S.; Dubey, S.; Gautam, R. K.; Chattopadhyaya, M. C.; Sharma, Y. C. Adsorption Characteristics of Alumina Nanoparticles for the Removal of Hazardous Dye, Orange G from Aqueous Solutions. *Arab J. Chem.* **2019**, *12* (8), 5339–5354.